Quantum Electronics **38** (12) 1083 – 1096 (2008)

INVITED PAPER

PACS numbers: 42.55.Px; 42.60.Da; 42.60.Fc; 42.60.Jf; 42.65.Ky
DOI: 10.1070/QE2008v038n12ABEH013965

Power scalable semiconductor disk lasers for frequency conversion and mode-locking

O.G. Okhotnikov

Abstract*. The semiconductor disk laser, a relatively novel type of light oscillators, is now under intensive development. These lasers produce an excellent beam quality in conjunction with a scalable output power. This paper presents recent achievements in power scalability, mode-locking and frequency conversion with optically-pumped semiconductor disk lasers. A novel concept for power scaling described here allows the thermal load of the gain material to be reduced, increasing the threshold of rollover and extending the capability for boosting the output power without degradation in the beam quality. The proposed technique is based on the multiple gain scheme. The total power of over 8 W was achieved in dual-gain configuration, while one-gain lasers could produce separately up to 4 W, limited by the thermal rollover of the output characteristics. The results show that the reduced thermal load to a gain element in a dual-gain cavity allows extending the range of usable pump powers boosting the laser output. Orange – red radiation required for a number of challenging applications can be produced through frequency-doubling using a GaInNAs/GaAs laser. Using such a disk laser operating at a fundamental wavelength of 1224 nm, we demonstrate an output power of 2.68 W in the visible region with an optical-to-optical conversion efficiency of 7.4 %. The frequency-converted signal could be launched into a single-mode optical fibre with 70 % – 78 % coupling efficiency, demonstrating good beam quality for the visible radiation. Using a Fabry – Perot glass etalon, the emission wavelength could be tuned over an 8-nm spectral range. We report on optically-pumped disk lasers passively mode-locked with a semiconductor saturable-absorber mirror. The potential of harmonic mode-locking in producing pulse trains at multigigahertz repetition rates has been explored. The mode-locked disk laser is investigated for different designs of the gain medium that allow bistable mode-locking to be controlled. An explanation for hysteresis of mode-locking is given based on a laser model including saturable absorption and unsaturated gain in a semiconductor oscillator operating in pulsed regime.

O.G. Okhotnikov Optoelectronics Research Centre, Tampere University of Technology, P.O. Box 692 FIN-333101, Tampere, Finland; e-mail: oleg.okhotnikov@tut.fi

Received 20 August 2008; revision received 3 October 2008
Kvantovaya Elektronika **38** (12) 1083 – 1096 (2008)
Translated by O.G. Okhotnikov

Keywords: *semiconductor lasers, vertical external-cavity surface-emitting lasers, semiconductor disk lasers, nonlinear frequency doubling, visible light generation, passive mode-locking, generation of ultrashort pulses with a high repetition rate, optical bistability.*

1. Introduction

Semiconductor disk lasers (SDLs) also known as vertical external-cavity surface-emitting lasers (VECSELs) present a type of lasers whose concept is based on the use of an optically-pumped semiconductor reflective structure as the gain medium inside a bulk optics cavity [1, 2]. A simplest linear cavity SDL using one spherical mirror as an output coupler is shown in Fig. 1a. These oscillators became attractive as they constitute a variation on the diode-pumped solid-state thin-disk lasers, with the advantage of a bandgap engineered emission wavelength.

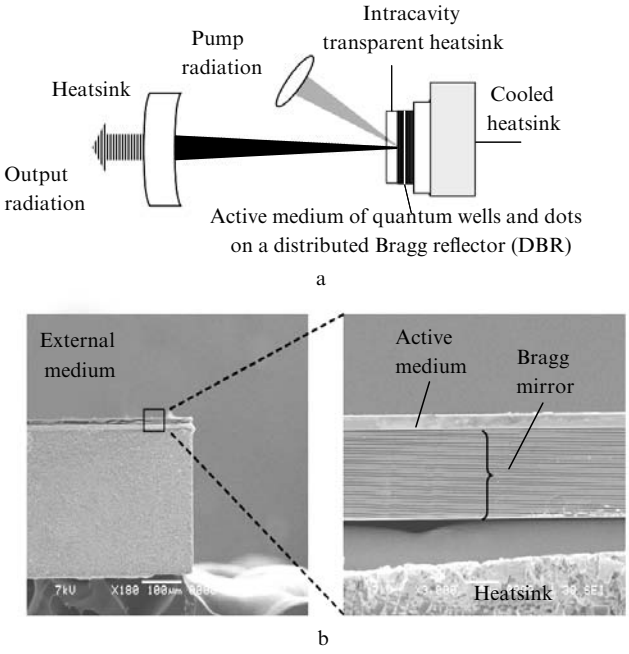

Figure 1. (a) Schematic setup of an SDL with linear cavity using one auxiliary spherical mirror. Semiconductor disk laser (SDL) consists of: semiconductor gain mirror (Gain region + Distributed Bragg Reflector, DBR), external output coupler and optical (or electrical) pumping. (b) Scanning electron microscope photos of cross-sectional view of the gain structure.

It is well known that the beam quality from surface-emitting lasers is far better than that obtained from in-plane edge-emitting diode lasers. An eminent example of such a surface-emitting laser is a vertical-cavity surface-emitting laser (VCSEL) which can generate a fundamental transverse mode beam, however, with a power typically limited to milliwatt level. Power scaling in monolithic VCSEL by increasing the output aperture is restricted to diameter of 10 μm to prevent a multimode oscillation. The need for high-power semiconductor lasers with good beam quality triggered the development of the new category of lasers – semiconductor disk lasers.

The extended laser cavity with external spherical mirror(s) allows one to boost the output power significantly, while preserving the fundamental transverse mode operation. This cavity configuration has demonstrated the highest power achieved from surface-emitting semiconductor lasers [3].

The semiconductor reflector provides the gain in the SDL in a direction normal to the wafer surface. SDL gain structure includes four sub-sections: a mirror, a gain section with quantum-wells (QWs) or planes of quantum-dots (QDs) as active element, a carrier-confinement window and a cap layer to protect the uppermost layer and those underneath from oxidation. The compositions and thicknesses of the different layers are typically chosen based on the lattice-bandgap energy diagram, reflectivity and field pattern to ensure its strong interaction with gain medium. Figure 2a shows variations in the refractive index and electrical field across the gain structure.

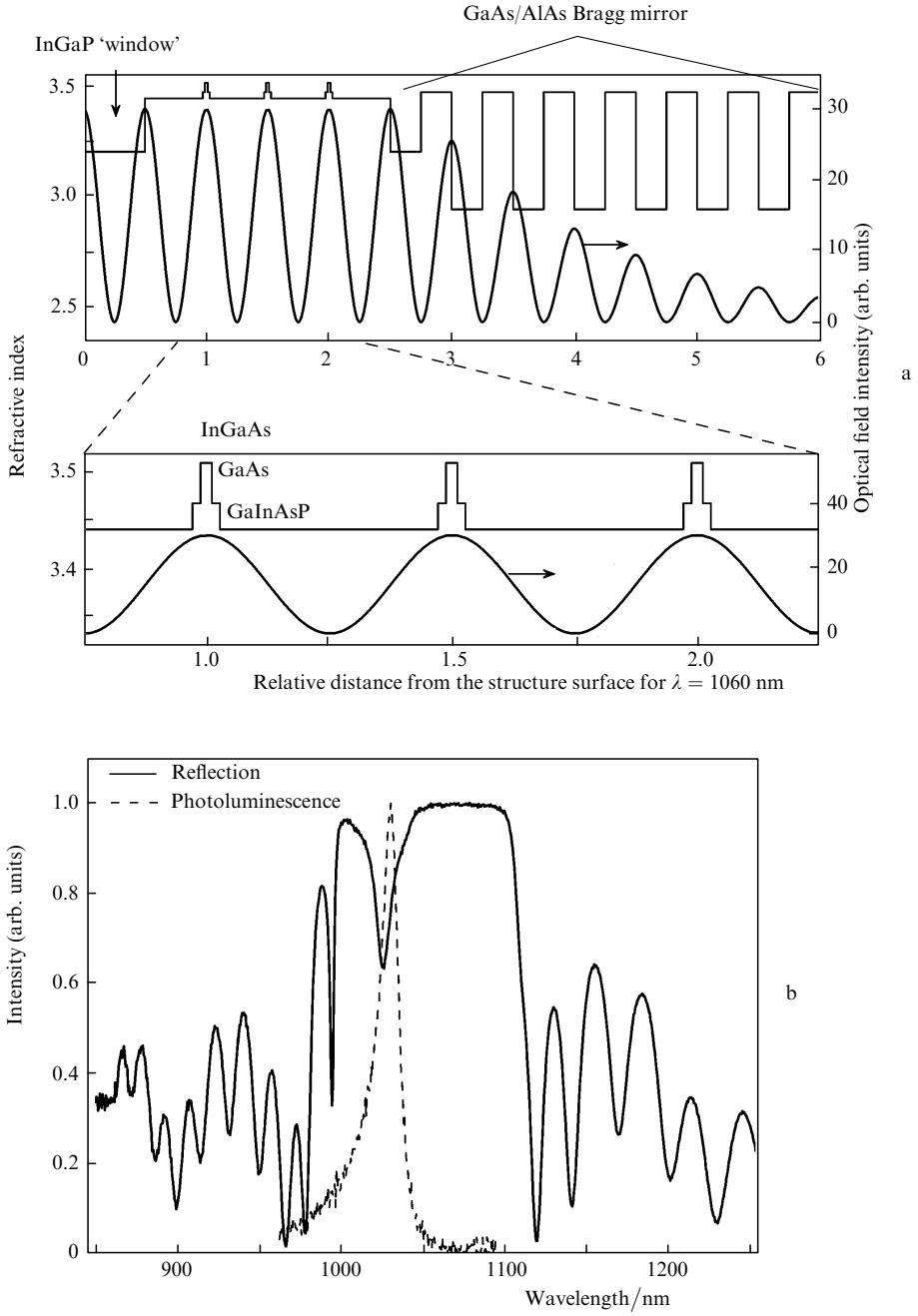

Figure 2. (a) Layout of a three quantum-well structure shows the refractive index and calculated standing wave intensity pattern for 1060 nm and (b) low-intensity reflectivity and photoluminescence spectrum of the gain reflector.

To maximise gain extraction from small thickness gain layers, e.g. QWs, they are typically placed at the antinodes of the standing-wave of the electric-field pattern established by the semiconductor mirror. This arrangement is known as resonant periodic gain (RPG) and illustrated in Fig. 2a [4]. The final part of the SDL structure is the confinement window. This layer is generally added to prevent pump-generated carriers from reaching the surface where they would be lost due to nonradiative recombination. The window layer should be transparent for both pump and signal radiation and to provide a sufficient electronic barrier for the carriers. Thickness adjustments of this layer are also often used to position the subcavity resonance resulting from the Fabry–Perot interference between the semiconductor surface and the DBR. Figure 2b shows typical low-intensity reflectivity and photoluminescence spectrum of the gain reflector.

In this paper, we present results of recent efforts in developments of SDLs with improved power scalability, mode-locked operation and frequency conversion.

2. Power scalable semiconductor disk laser using multiple gain cavity

Concept of the scaling technique. Though it is well established that optically pumped semiconductor disk lasers can produce high power with a good quality of the beam, both parameters are critically dependent on the efficiency of the heat removal from the gain structure operating under strong pumping condition [4–7]. Heat spreaders with high thermal conductance, e.g. diamond, SiC or copper, providing efficient heat dissipation, should be used in high power SDLs to reduce rollover and thermal lensing]. Although, the technology of the wafer bonding and heat spreaders constantly improves, the beam quality and output powers achievable from SDL would eventually be limited by the state-of-the-art of the thermal management. In order to increase the SDL power, a number of approaches have been considered. The power scaling could obviously be achieved by increasing the mode size on the gain medium, however, some penalty to the beam quality can generally be expected [4]. It is also possible to distribute the pump power into a number of spots over the gain structure forming arrayed or 'parallel' geometry. The resulted increase in the output power would, however, correspond to the multiple beams with a complicated spatial distribution. With gain segments formed on a large semiconductor chip and connected in series by the multi-bounce cavity, the fundamental-transverse mode with increased output power could be expected [2, 8]. This geometry, however, uses a single heatsink, which may limit efficiency of heat extraction and is difficult to implement practically.

To cope with this problem, we propose the design with two entirely separated gain elements with individual heat-spreaders placed in the same cavity for power scaling, while preserving the high quality of the output beam. In principle, the concept can be applied to a number of gain elements. The multiple gain cavity could take on higher pump powers by sharing thermal load among different gain elements thus avoiding excessive heating and the rollover. It should be mentioned that a similar approach was demonstrated to be attractive for solid-state disk lasers [9, 10]. The results show impressive power scalability up to 1 kW, however, with compromised beam quality.

Gain material and laser setup. The laser structure was designed for operation around 1050 nm and it comprises a 30.5-pair GaAs/AlGaAs distributed Bragg reflector and a gain section with 13 non-strain-compensated $Ga_{0.74}In_{0.26}As$ quantum-wells grown monolithically on a GaAs substrate by molecular beam epitaxy. In order to improve the heat transfer from the gain section, transparent diamond heat spreaders of 300-μm thickness were capillary bonded on the top of the 2.5×2.5 mm gain samples [11, 12]. The gain samples were mounted in water-cooled copper heat sinks. The diamond–air interface was coated with a two-layer $TiO_2 - SiO_2$ film to reduce pump and signal reflection. The Z-shaped laser cavity was defined by the two semiconductor gain mirrors, a curved 5 %-output coupler mirror and a high reflective spherical folding mirror. The laser setup is shown in Fig 3. The gain structures were optically pumped at 800 nm with multimode fibre-coupled diode systems at an angle of about 35°. The pump spot diameter on both gain media was about 180 μm, which matches the fundamental mode size of the cavity expected from numerical simulation. During all measurements, the temperature of the copper mounts was kept at 15 °C.

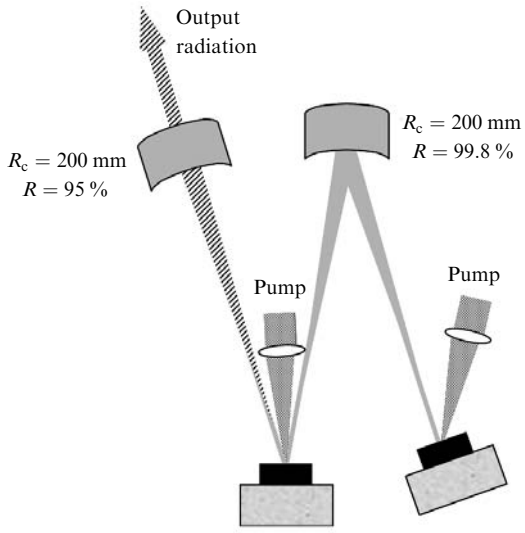

Figure 3. Semiconductor disk laser with the cavity including two separate gain reflectors and two curved mirrors. R_c is the radius of curvature, R is the reflectivity.

Results. The output characteristics, spectrum and beam quality factor M^2 were measured from the dual-gain laser and two lasers each using single-gain element. The performance of each gain mirror was tested in a single-gain cavity with output coupling of 3 %. The lasers were operated with the central wavelength near 1050 nm. Light output characteristics, shown in Fig. 4, demonstrate that power achieved from the dual-gain laser is increased by a factor of two compared to a single-gain setup.

This result indicates that the thermal load on the gain structures in the dual-gain configuration is reduced compared to a one-gain laser pumped with the same power. Consequently, the thermal rollover in a single-gain scheme limits usable pump power and prevents power scaling. On the contrary, the dual-gain laser has an increased threshold of the thermal rollover and allows for significant power scaling.

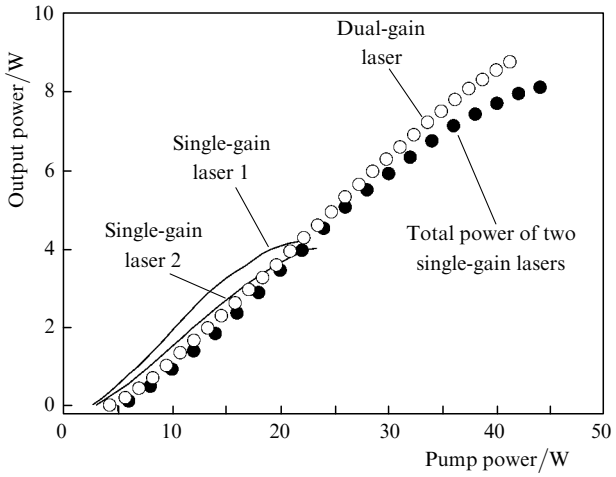

Figure 4. Light output characteristics of dual-gain laser, single-gain lasers, and sum of the single-gain laser outputs versus total pump power.

The beam quality factor M^2 was measured for orthogonal directions using an automated scanning slit device. For single-gain lasers, the M^2 parameter was 1.2 in both directions at the maximum power. The dual-gain disk laser reveals good beam stability with the output power indicating only a minor increase in the M^2 factor by 15 % – 20 % up to 1.28/1.45 at the output power of 8 W. The spatial beam distribution fitted with a Gaussian distribution is shown in Fig. 5.

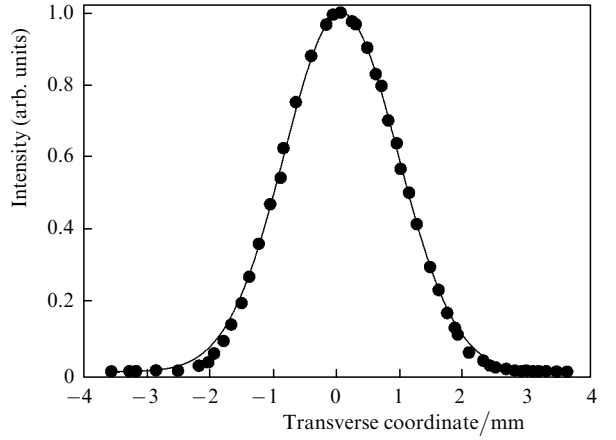

Figure 5. Intensity profile of the output beam and Gaussian fit of the two-gain laser at output power of 8 W.

3. Visible light generation from SDL using intracavity frequency doubling

High power lasers emitting at visible wavelengths are needed for a number of applications including optical pumping, life sciences and laser projection displays. Multi-watt visible emission has been produced from frequency-doubled semiconductor disk lasers at blue [13], green [14] and yellow [15] wavelengths using the InGaAs/GaAs material system. Recently, direct generation of red emission at 674 nm from a GaInP-AlGaInP/GaAs-based source pumped by a green solid-state laser [16] was demonstrated. However, it is increasingly difficult to extend the GaInP technology towards wavelengths below 635 nm, because of a lack of suitable direct bandgap barrier materials that would provide sufficient carrier confinement in the quantum wells. On the other hand, increased lattice mismatch between InGaAs and GaAs hinders the use of this materials system at the wavelengths above 1180 nm that are needed for generation of amber emission through frequency-doubling. Gerster et al. have demonstrated a frequency-doubled orange-red (610 nm) source based on GaAsSb/GaAs material [17]. Alternatively, the conventional InGaAs technology can be extended to longer wavelengths by introducing a small amount of nitrogen into the crystal lattice, typically up to 3 %. Dilute nitride GaInNAs disk lasers operating at 1.3 μm have been reported previously [18]. Recently, we have obtained 615 – 617-nm emission from an intracavity frequency-doubled disk laser based on GaInNAs material [19 – 21]. Here, we demonstrate that dilute nitride semiconductor is suitable for generating multi-watt orange – red output with a high efficiency and a good beam quality.

The presented results illustrate how the combination of vertical-emitting semiconductor structures and intracavity nonlinear conversion techniques can be successfully exploited to meet demands for continuous-wave radiation in the application-rich visible spectral range.

Semiconductor structure and device processing. The gain mirror was grown by molecular beam epitaxy equipped with a RF-plasma source for incorporating the nitrogen into the semiconductor crystal. Apart from the quantum wells (QWs) and barriers composition, the gain mirror structure is typical for any semiconductor disk laser. It includes a high reflective Bragg stack and a multiple quantum wells gain region grown on an n-type GaAs substrate. The distributed Bragg reflector (DBR) was comprised of 30 pairs of $\lambda/4$-thick AlAs/GaAs layers. The active region included ten 9-nm-thick GaInNAs QWs uniformly distributed in five pairs. For strain compensation/mediation we used 4-nm-thick GaAsN layers surrounding each QW. Pump absorbing GaAs spacer layers were used to position the QW pairs in-line with the antinodes of the standing wave formed between the DBR and semiconductor – air interface. A large bandgap AlGaAs window layer was grown on top of the gain section to avoid nonradiative recombination of photocarriers at the surface of the gain mirror. The structure was completed with a thin GaAs layer that protects the window layer from the oxidation.

Since the gain mirror operates under intense pumping conditions, thermal management is a crucial issue for the disk laser. In our laser the generated heat was conducted to a heat sink using a transparent intracavity heat spreader. A 2.5×2.5-mm laser chip was scribed from the as-grown wafer and capillary bonded with de-ionised water to a $3 \times 3 \times 0.3$-mm natural type IIa diamond heat spreader. In this bonding technique [11, 12], two flat and smooth surfaces are pulled into close contact by the surface tension of water, methanol or another suitable liquid, and bonded together by intermolecular surface forces. The bonded component was assembled between two metallic plates with indium foil in between to ensure good thermal and mechanical contact. The topmost metal plate had a circular aperture for signal and pump beams. The mounting assembly was cooled with circulating water down to 7 °C.

Experimental results. The laser includes the gain mirror and three curved mirrors forming a Z-type cavity, as shown

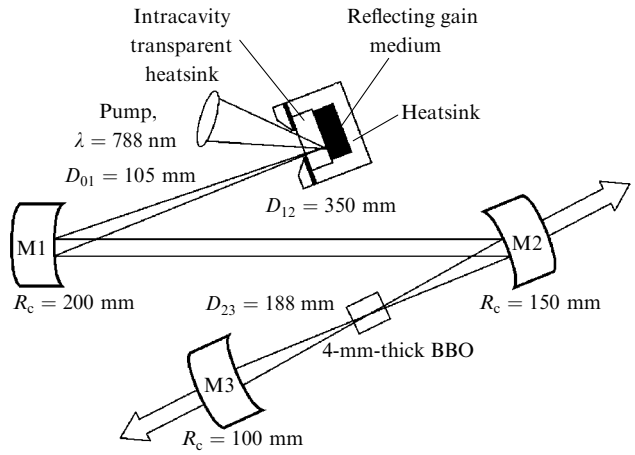

Figure 6. Experimental setup, consisting of three curved mirrors and the gain mirror forming a Z-cavity. The output light was coupled to an optical fibre located behind mirror M3. *D* is the distance between mirrors.

in Fig. 6. All curved mirrors are highly reflective for the fundamental wavelength of 1.2 μm and have transmission over 90 % for the second-harmonic radiation. The gain medium was pumped with a fibre-coupled 788-nm pump diode laser at an angle of 35° to the surface normal of the gain mirror. The cavity was designed to match the size of the laser mode with the 290-μm diameter of the pump spot at the gain mirror. A 4-mm long nonlinear BBO crystal was placed between mirrors M2 and M3 in the waist of the cavity transverse mode. The waist diameter was calculated to be approximately 160 μm with a Rayleigh length of 18 mm. The BBO crystal was critically, type-I, phase matched and antireflection coated for 1220 nm and 610 nm on both facets. Red emission appears as two beams behind mirrors M2 and M3. In order to measure the output power at different wavelengths independently, the residual infrared power was spatially separated from red emission with a dichroic beam splitter.

The laser radiation was delivered to an optical spectrum analyzer using a multimode fibre. The corresponding frequency-doubled spectrum at 612 nm is presented in Fig. 7. The output characteristic of the laser is presented in Fig. 8a. The total output power from mirrors M2 and M3

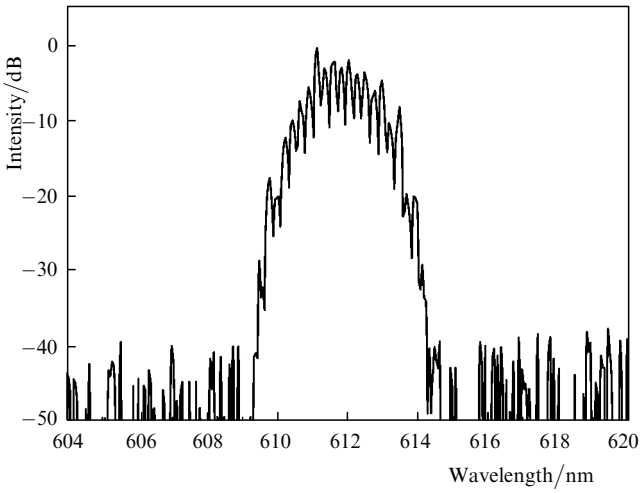

Figure 7. 612-nm frequency-doubled spectrum.

was 2.68 W at 612 nm with the absorbed pump power of 36.1 W. The measured total power at the fundamental wavelength of 1224 nm that leaked from the cavity was negligible. The conversion efficiency into the red emission was 7.4 %. The polarisation of the fundamental and the frequency-doubled beams was also studied. The outputs at both wavelengths, shown in Fig. 8b, are plotted as a function of the polariser angle and indicate that the signals are linearly polarised in orthogonal directions.

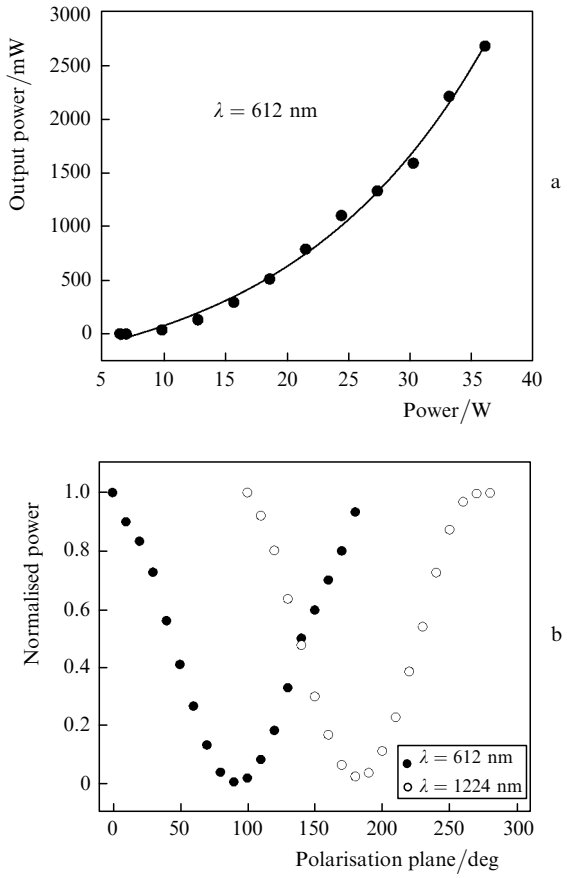

Figure 8. (a) Output characteristic of the laser showing frequency-doubled power as a function of pump power. The value of pump power used in this plot takes into account the fraction of the light reflected (~ 17.6 %) from the surface of the bonded sample. Nearly 2.7 W of visible radiation has been achieved. The total power leakage from the cavity at 1224 nm was found to be negligible. (b) Normalised power as a function of the polariser angle showing that fundamental and frequency-converted beams are linearly polarised in orthogonal directions.

Spectrally narrow-line operation was achieved with a 25-μm solid glass etalon inserted in the cavity. The etalon was placed between mirrors M1 and M2. The tuning range at the fundamental wavelength was 16 nm, limited by the free-spectral range of the Fabry–Perot glass etalon. The corresponding tuning range in the visible was 8 nm, as presented in Fig. 9.

The beam profile of the red emission was studied with a CCD-camera. The transverse beam profiles are shown in Fig. 10a. The beam was found to be slightly elliptical with a Gaussian profile for both directions. The ellipticity is likely to originate from spatial walk-off in the BBO crystal. In order to quantify the quality for the elliptical beam, we launched the red emission from the output to a fibre with

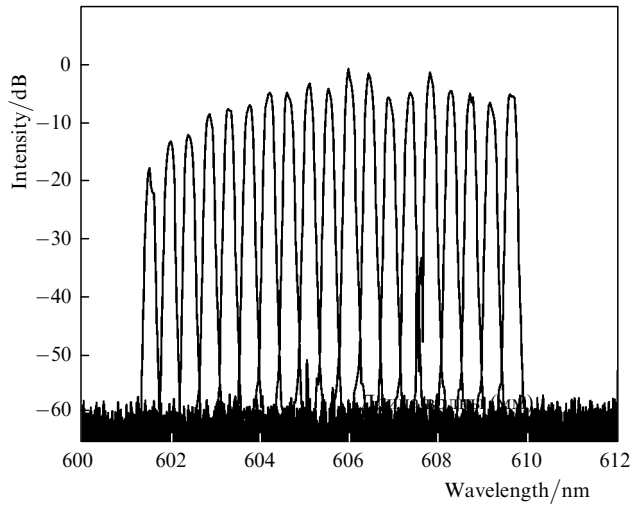

Figure 9. Narrow-line tuning spectra at the red measured near the threshold. The tuning was achieved by tilting the 25-μm-thick Fabry–Perot glass etalon inside the cavity.

single-mode guiding in the visible and determined the coupling efficiency for different powers. The coupling efficiency into the fibre was 78 % at low power and gradually decreased down to 70 % with an increase in the output power. Coupling efficiency as a function of the output power at 612 nm is shown in Fig. 10b. Efficient coupling to a single-mode fibre indicates that despite the elliptical shape, the output beam corresponds to nearly single-transverse-mode, with very moderate beam quality degradation with the increasing output power.

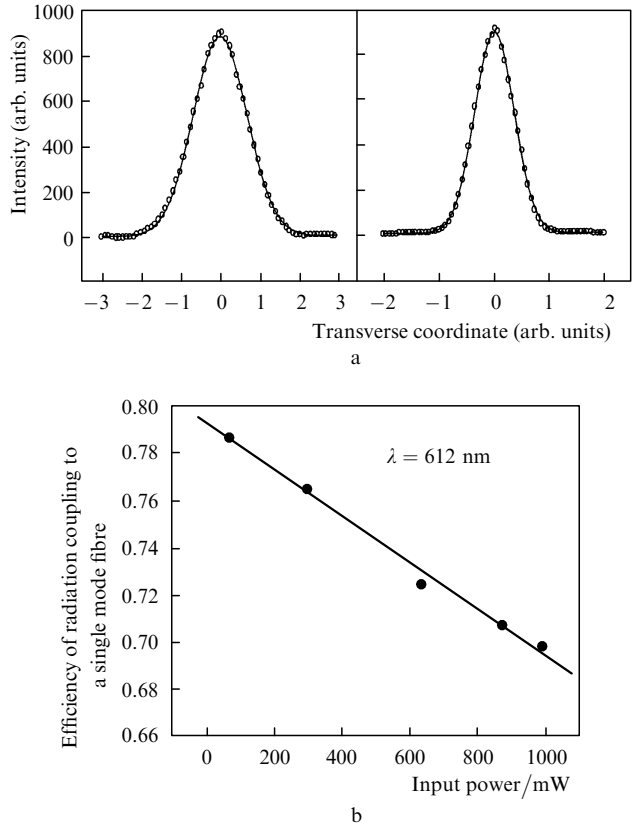

Figure 10. (a) Transverse beam profile of the red beam, with a Gaussian fit in vertical and horizontal directions. (b) Coupling efficiency to a single-mode fibre as a function of the output power at 612 nm from at the output.

4. Harmonically mode-locked SDLs for multi-GHz pulse train generation

SDLs passively mode-locked with semiconductor saturable absorber mirrors (SESAMs) use the broad gain bandwidth of the quantum-well material for generation of ultrashort pulses and can achieve gigahertz-level repetition rates in a short cavity (5–10 cm) or through harmonic mode-locking. SDLs operating at high repetition rates (tens of gigahertz) can be used in high-speed communications, switching, sampling, and clocking. Since solid-state or glass fibre laser gain media have a low emission cross section and high saturation fluence, these lasers may suffer from Q-switching instability particularly for high repetition rate mode-locking. In contrast, SDLs have a high differential gain, low saturation fluence and are free from low-frequency instabilities even with low energy pulses. Multi-GHz (10–100 GHz) SDLs reported to date were using short cavities [22, 23] or external feedback to provoke harmonic mode-locking [24]. The mechanisms of high-repetition-rate pulse formation in SDLs, especially harmonically mode-locked, are still to be thoroughly studied.

In this chapter, we present the results of the systematically study of the harmonic mode-locking regime in SDLs and demonstrate the main features associated with this operation mode. Particularly, we show both numerically and experimentally, that harmonic mode-locking is inherent in SDLs; the number of pulses circulating in the cavity is expected to increase with pump power. Strong saturation and fast recovery of the gain ensure efficient pulse ordering mechanism resulting in strong suppression of cavity fundamentals.

SDL gain mirror, SESAM and laser cavity. The GaAs-based laser gain structure consists of a quantum well gain section enclosed between a GaInP etch-stop layer and a distributed Bragg reflector (DBR). The structure was grown in a single step by molecular beam epitaxy (MBE). The gain section contains 15 compressively strained 7-nm-thick GaInAs quantum wells sandwiched between 5-nm-thick GaAs barrier layers and spaced with strain compensating GaInAsP layers. The thickness of the spacers was set to place each QW at an antinode of the optical field in the 8.75λ-long cavity defined by the DBR and the semiconductor–air interface. The distributed Bragg reflector includes 27.5 pairs of $\lambda/4$-thick GaAs/AlAs layers and was grown last on top of the gain section.

The sample was attached with indium solder on a $2 \times 2 \times 0.3$ mm diamond composite heat spreader, which in turn was bonded to a metallic heatsink with AuSn solder. After bonding, the GaAs substrate was removed using wet etching and a 2-layer $SiO_2 - TiO_2$ antireflection coating was deposited on the sample.

The gain mirror was pumped by 808-nm radiation from a fibre-coupled diode focused onto a spot of about 165-μm in diameter. The barrier and spacer layers absorb the pump radiation creating the carriers that are trapped in the wells to generate gain at 1 μm.

The SESAM used as an end mirror in the mode-locked laser was grown by MBE. It comprises two 9-nm-thick

compressively strained GaInAs quantum wells separated by a 5-nm-thick GaAs barrier and a GaAs/AlAs DBR with 27.5 pairs of quarter-wave thick layers. Figure 11 shows the low-intensity reflectivity of the SESAM. The SESAM has been irradiated with heavy ions to shorten the recovery time of the absorption. The recovery time estimated from measurements was found to be 2 ps. Low single-pass gain in a SDL makes the cavity extremely sensitive to the cavity loss. Consequently, the modulation depth of the SESAM was limited here to 1 %. This value, however, was sufficient to ensure reliable triggering of the passive mode-locking. The saturation fluence of the SESAM was measured to be 50 μJ cm^{-2}.

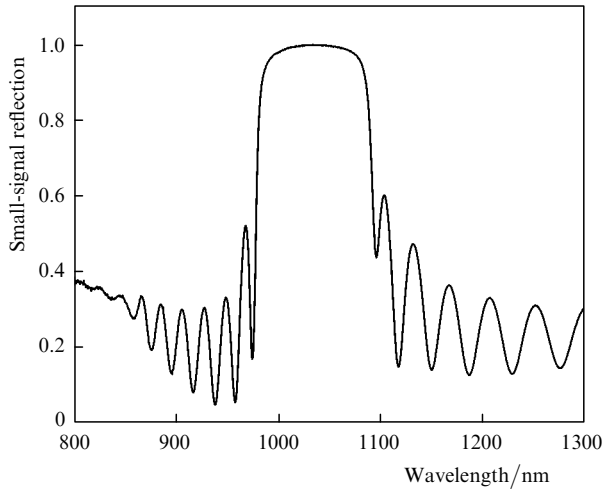

Figure 11. Low-intensity reflectivity of the SESAM.

The asymmetric Z-shaped laser cavity, shown in Fig. 12, consisted of two curved folding mirrors and two semiconductor end-mirrors represented by the gain structure and the SESAM. This configuration provides a convenient option for setting the suitable mode size on the gain mirror and the absorber.

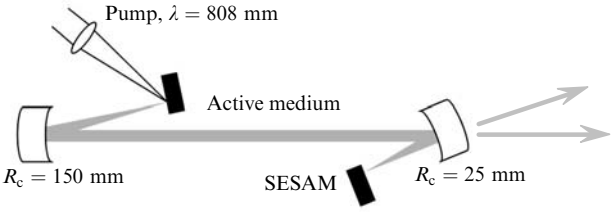

Figure 12. Cavity setup of the mode-locked SDL.

To achieve stable mode-locked operation, the mode area on the SESAM should be usually smaller than the mode area on the gain structure optimised to match the pump spot [25]. An optical isolator was placed at the output of the laser to prevent back-reflection to the laser.

Mode-locking characteristics. The laser described above typically generated 10 – 20 ps pulses at a wavelength between 1036 and 1040 nm, depending on pump power and the number of pulses circulating in the cavity.

Figure 13 shows the radio-frequency spectra of the current from a photodiode with bandwidth of 12 GHz illuminated with the output laser beam for several pump powers corresponding to different harmonics. The strong (> 50 dB) suppression of the cavity fundamentals (multiples of 350 MHz) indicates that the pulses are nearly equally spaced. In turn, this illustrates the high strength of the pulse ordering mechanism in passively mode-locked SDL. It should be noted that highly periodical pulse trains are desirable in many applications, therefore enhancement of the intrinsic mechanism of pulse ordering observed in SDL and studied here is an important issue.

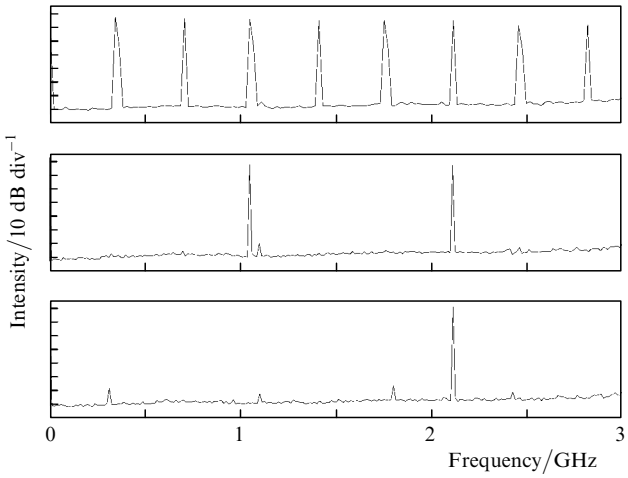

Figure 13. RF-spectra for the fundamental (top diagram), 3rd and 6th harmonics. Spectra were measured with a 12-GHz photodiode.

Another feature observed regularly in the mode-locked SDL is an increase in the order of the oscillating harmonic with pump power. It was found that the number of pulses circulating in the cavity increases fairly linearly with pump power, as shown in Fig. 14. This observation is in agreement with the theoretical model described below that confirms gradual increase in harmonic number with the pump power. The marker bars around data points in Fig. 14 denote the pump power range for the stable mode-locked operation of a given harmonic.

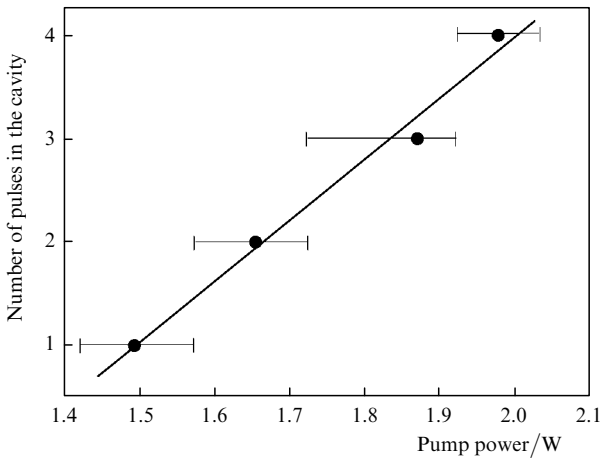

Figure 14. Number of pulses circulating in the SDL cavity as a function of the pump power.

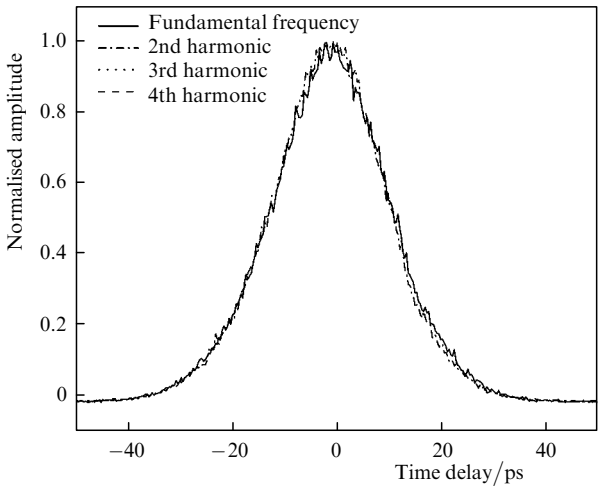

Figure 15. Pulse autocorrelations for different number of pulses circulating in the laser cavity.

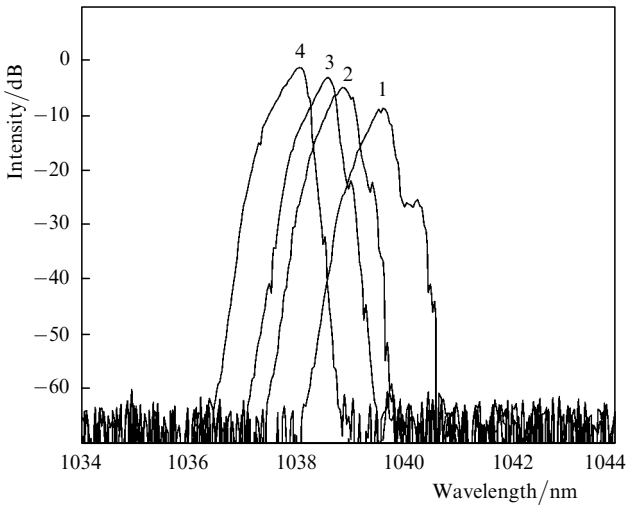

Figure 17. Laser spectra for different number (1–4) of pulses inside the laser cavity.

The autocorrelation traces of the pulses corresponding to different harmonics are shown in Fig. 15. The pulse width gradually decreases from 16.3 to 14.8 ps with an increase in the harmonic order, as seen from Fig. 16.

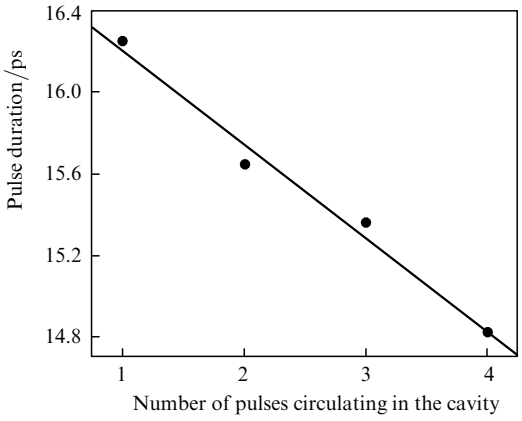

Figure 16. Dependence of the output pulse duration on their number in the cavity.

The corresponding spectra are shown in Fig. 17. In these measurements, the time-bandwidth product ranges from 1.5 to 1.9 exceeding the transform-limited value by factor of 5–6. The pulse energy was fairly constant revealing only a minor increase with increasing harmonic number from 38 pJ to 42 pJ.

The pulses generated by the passively mode-locked SDLs acquire usually frequency chirp as a result of complex interplay between nonlinearity (phase effects) and saturation of the gain and absorption [25]. The pulses could, however, be compressed close to the diffraction limit using an auxiliary delay line with anomalous dispersion. We have found that using a diffraction grating pair allowed for subpicosecond pulses with time-bandwidth product only slightly above the transform limit. Another possibility for producing chirp-free pulses directly from the mode-locked laser could be based on the 'quasi-soliton' formation in the positive-dispersion regime and was discussed in [25].

The blue spectral shift observed with an increase in harmonic number shown in Fig. 17 could be understood from the dynamic gain/absorption saturation model, as shown in [26]. At high repetition rate (>1 GHz), when the gain cannot be fully recovered during the pulse period, a decrease in the time-bandwidth product has been observed with an increase in the repetition rate (harmonic number), as shown in Fig. 18. The decrease in the frequency chirp induced by the gain saturation is expected with a weaker recovery of the gain for high pulse repetition rates.

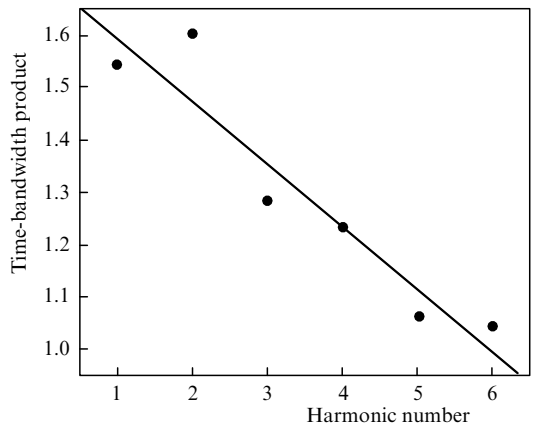

Figure 18. Time-bandwidth product dependence on harmonic number (number of pulses circulating in the laser cavity).

Numerical model. Strong repulsing or pulse interaction is needed to establish equal spacing between the pulses. The saturation and fast recovery of the gain are believed to be the main mechanisms responsible for pulse ordering in a harmonically mode-locked SDL. The ordering mechanism was investigated using the numerical simulations based on rate equations for the saturable gain and saturable loss. The simulations assume that the saturable absorber is highly oversaturated, which corresponds to experimental conditions.

The saturation of the gain g in the SDL is described by the rate equation in a form [25]

$$\frac{dg(t)}{dt} = -\frac{g(t) - g_0}{\tau_g} - \frac{g(t)P(t)}{E_{sat,g}}. \quad (1)$$

The saturable absorption q is found from equation [25]

$$\frac{dq(t)}{dt} = -\frac{q(t) - q_0}{\tau_a} - \frac{qP(t)}{E_{sat,q}}, \quad (2)$$

where t is the time; q_0 is the modulation depth; g_0 is the small-signal gain, which is proportional to the pump power; τ_g and τ_a are the recovery times; and $E_{sat,g}$ and $E_{sat,q}$ are the saturation energies for the saturable gain and saturable loss, respectively; and P is the pump radiation power. The model includes a dispersive element that accounts for the second-order chromatic dispersion and gain filtering. The propagation through this element is carried out by a multiplication in the frequency domain:

$$\tilde{E}_b(\omega) = \exp\left(\frac{i}{2}D_2\omega^2\right)\exp\left[-\left(\frac{\omega}{\omega_g}\right)^2\right]\tilde{E}_a(\omega).$$

Here, $\tilde{E}_a(\omega)$ and $\tilde{E}_b(\omega)$ are the Fourier transforms of the slow-varying electric-field amplitude before and after the dispersive element, respectively; ω is the frequency; D_2 is the dispersion; and ω_g is the gain bandwidth. The simulations start from low-amplitude white noise. The bandwidth for the gain filtering was set to $\tau_{pulse} \sim 0.0015T_r^{-1}$, where T_r is the cavity round-trip time. This resulted in pulse durations ($\tau_{pulse} \sim 0.0015T_r^{-1}$) consistent with the experimental data.

To match closely the laser parameters, the recovery time of the gain was set to be equal to the cavity round-trip time, $\tau_g = T_r$ (both characteristic times are of the order of 1 ns for our laser) and the recovery time of the SESAM to be $\tau_a = T_r/100$. The gain saturation energy was assumed to be 100 times the SESAM saturation energy. The saturable loss of the SESAM was set to 2 % and additional losses of 6 % have been included representing the cavity loss and output coupling. The model was completed by α-factors, which account for phase effects proportional to the saturable gain ($\alpha_{gain} = 2$) or loss ($\alpha_{SESAM} = 1$) [22]. Figure 19 shows the time dependence of the pulsed output, SDL gain and the saturable absorption obtained from the simulations performed for 40000 round trips starting from white noise. The simulations reveal that saturable gain results in a temporal pulse shift per round trip of the order of $3 \times 10^{-6}T_r$, while the difference of the time shift between the strongest and the weakest pulses is $1 \times 10^{-6}T_r$. These values correspond to the non-steady-state of the harmonic mode-locking after 40000 round trips. Calculations show that both values approach zero after 60000 round trips indicating the formation of the steady-state of the harmonic mode-locking. The arrows in Fig. 19(a) indicate direction and relative magnitude of the pulse temporal shift caused by the SDL gain recovery. The saturable absorber cannot contribute to the pulse ordering process due to its fast recovery and the large pulse separation.

The effect of cavity dispersion was then studied by adding negative or positive dispersion of the value of $2.0 \times 10^{-9}T_r^2$. Without soliton shaping, the pulse duration is expected to be independent of the sign of dispersion due to the low values of the amplitude-dependent phase effects in the semiconductor materials [25, 27]. This resulted in an increase of the pulse width from $\tau_{pulse} = 0.0015T_r$ to $\tau_{pulse} = 0.003T_r$. The pulse ordering mechanism, however, was found to be fairly independent of the cavity dispersion.

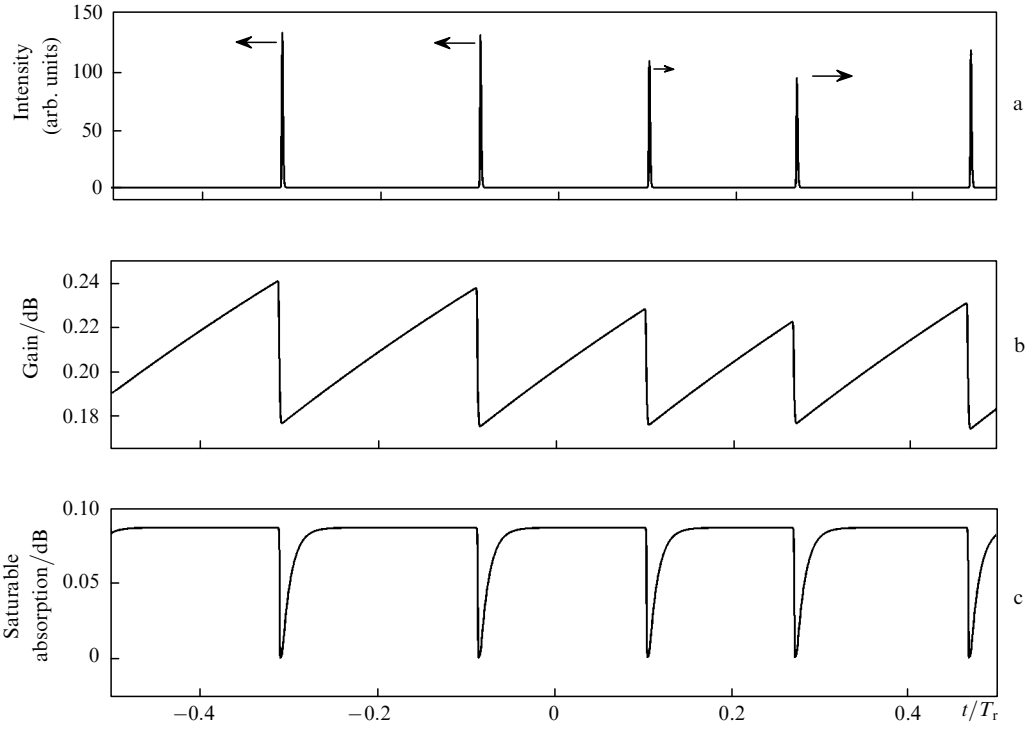

Figure 19. Dynamic evolution of the mode-locked SDL parameters. The time span corresponds to one round trip T_r: (a) the pulse waveform, (b) the corresponding SDL gain and (c) the saturable absorption. The arrows in (a) indicate the direction of the temporal pulse shift caused by the gain recovery. The length of the arrows is a measure of the pulse ordering strength. The pulse shift is measured with respect to the average time shift.

The laser considered here operates essentially in the non-soliton regime, contrary to the multiple pulse model used in [28]. This conclusion is supported by the large time-bandwidth product of the pulses observed in the experiments. Consequently, the pulse quantization owing to soliton pulse formation [29] does not occur here and the steady-state pulse energy is determined mainly by the gain saturation and cavity loss.

Figure 20 shows the number of ordered pulses in the laser cavity as a function of relative pump power obtained from numerical simulations. One can see from this figure that the number of pulses increases linearly with increasing pump power in accordance with the experimental results presented in Fig. 14. Estimates of the nonlinear phase effects in the laser cavity derived from numerical simulations show that phase shifts associated with the saturation of the gain and SESAM absorption affect mainly the pulse width and quality, but they can be neglected when considering multiple-pulse ordering in the harmonically mode-locked SDL. Briefly, due to time-dependent gain, the pulse shifts on a time scale towards the region with higher gain resulting in pulse ordering [25]. The strength of the drift force depends on the temporal gain slope $\partial g/\partial t$, which, in turn, depends on the gain magnitude and recovery time and pulse interval.

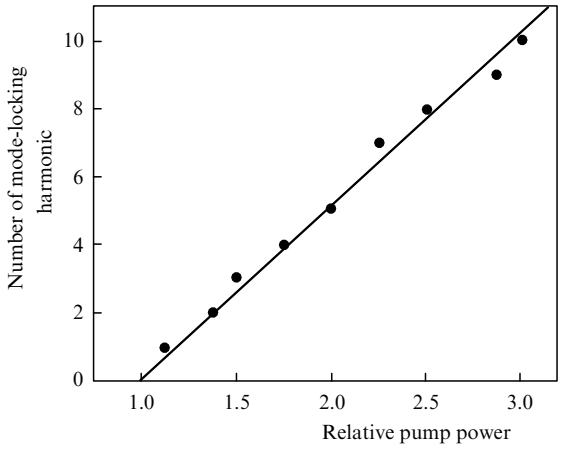

Figure 20. Number of mode-locking harmonic versus pump power found from numerical simulations.

The pulse energy distributions in the laser cavity after 10^5 and 1.3×10^6 round trips are presented in the Figs 21a and c, respectively. Figure 21b illustrates the evolution of the pulse ordering by plotting the temporal position of the pulse as a function of round-trip number. After 10^6 round-trips from the mode-locking start-up, the pulse amplitude variation decreases from 40 % to 2 %, while uncertainty in the temporal pulse location started from 40 % becomes negligible. It was found that adding either negative or positive dispersion to the cavity does not affect notably the pulse ordering mechanism, resulting both in a well ordered state after 10^6 round trips in the cavity.

The model described here implies ways to control the pulse energy and multiple pulsing. For instance, increasing the recovery time of the gain and absorber would reduce the pulse number. In contrast, the harmonic number can be increased using materials with shorter recovery times. The pulse energies can be scaled up by increasing the saturation

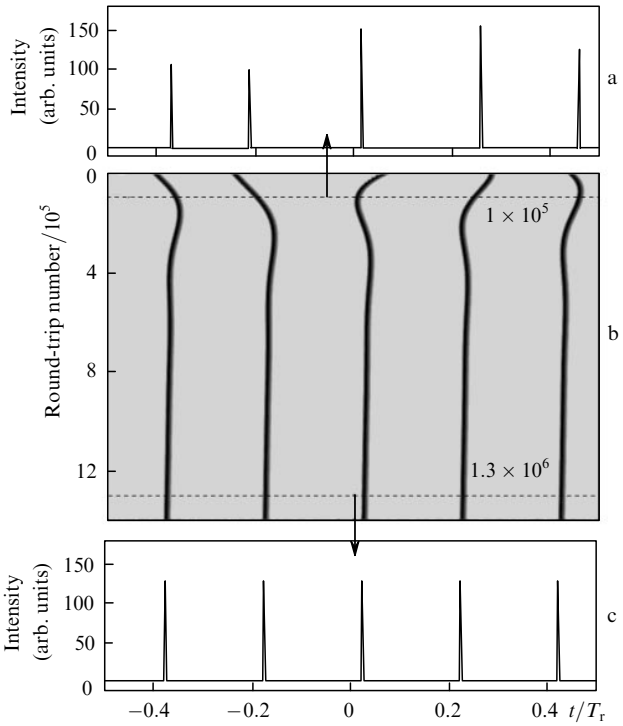

Figure 21. Evolution of 5th-harmonic mode-locking in a SDL. (a) The pulse power distribution after 10^5 and (c) after 1.3×10^6 round trips. Plot (b) shows the evolution of the pulse position with the round trip number. The power is given in [gain saturation energy/round-trip time] ratio and time is normalised to the round-trip time.

energies, e.g. by increasing the beam spot sizes on both the absorber and the gain material.

Hysteresis and bistability of multiple pulsing in a semiconductor disk laser with a saturable absorber. It is generally expected that a laser with a saturable absorber can exhibit bistability in the output characteristics at the threshold [30, 31]. With an increase in the pumping rate from a sub-threshold state, the cavity losses exceeding the net gain, the radiation will eventually bleach the saturable absorption. The threshold condition can then be satisfied resulting in the initiation of the laser oscillation. With a decrease in the pump power, the absorption remains bleached as long as sufficient radiation density is stored in the cavity. This is a basic illustration of how hysteresis of the optical characteristics appears in a laser with a saturable absorber in the cavity.

The results presented here describe the first observation of the bistability and hysteresis in the output characteristics of a passively mode-locked semiconductor disk laser incorporating a saturable absorber mirror. The study is focused on the effect of the gain structure on the laser performance. Particularly we demonstrate that the regime of bistable mode-locking can be controlled by the strength of the light interaction with the quantum-well gain medium.

First, the gain medium with the resonant periodic gain (RPG) structure has been grown. The parameters of the gain structure and SESAM used in this study are similar to the characteristics of those described above.

The laser setup used in the experiment is shown in Fig. 22. The Z-shaped, 15-cm-long laser cavity is formed between the SESAM and a curved output coupler with a radius of curvature 50 mm. The semiconductor gain chip

and a curved high reflector serve as folding mirrors in the cavity. The 30-mm radius of curvature of the high reflector ensures tight focusing of the beam onto the SESAM. A fibre-coupled pump diode emitting at 808 nm is focused on a spot of ~ 165 μm to match the diameter of the mode. This setup was used throughout this study unchanged except for the output coupler, which was adapted for each gain medium exploited. Output coupling was 3 % when the uncoated resonant gain structure was employed. With the coated RPG and antiresonant structures, the output coupling was decreased to 1 % and 0.5 %, respectively, in order to compensate for the lower gain of these gain designs. The output beam passed through an optical isolator that prevented back-reflections to the laser. The output was monitored with an autocorrelator, an optical spectrum analyser and a fast (12.5 GHz) photodiode connected to an electrical spectrum analyser and a communications signal analyser. The pulse duration throughout this study ranged from 5 to 35 ps, depending on the output power and harmonic number, as described in [26, 32]. The fundamental pulse repetition rate was 1.03 GHz.

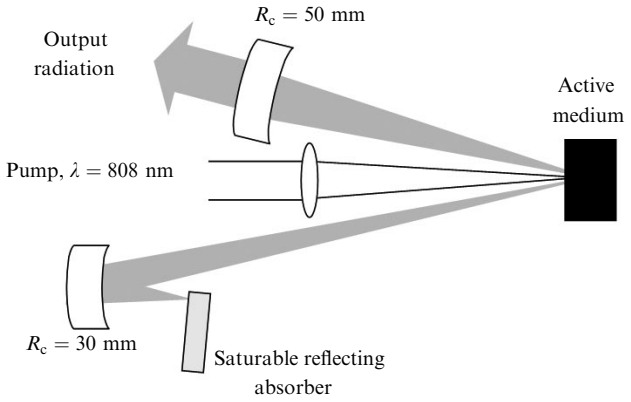

Figure 22. Schematic of a mode-locked disk laser.

The average output power is plotted in Fig. 23 as a function of pump power for the uncoated RPG gain

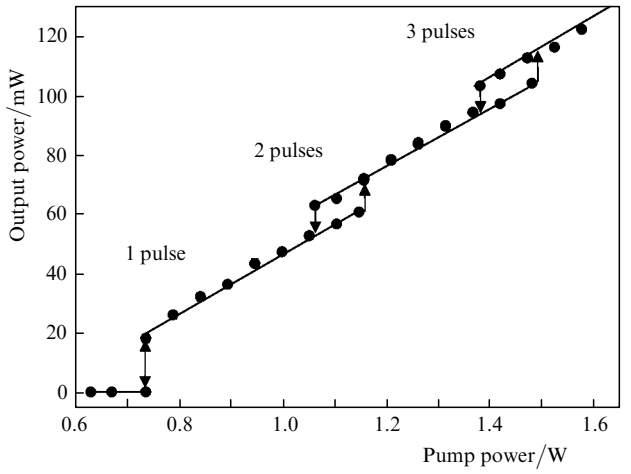

Figure 23. Output characteristics for the mode-locked disk laser using a resonant periodic gain medium. Operation at the fundamental, second and third harmonic frequencies has been achieved.

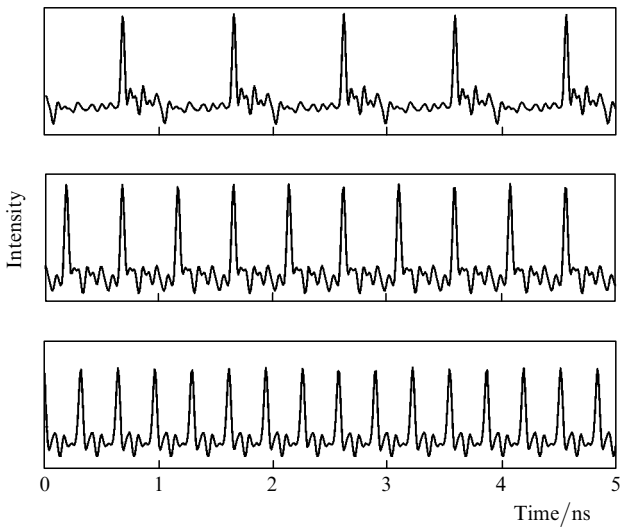

Figure 24. Oscilloscope traces of the mode-locked pulse sequence obtained for different pump power levels corresponding to the states illustrated in Fig. 23 with 1, 2 and 3 pulses circulating in the laser cavity.

medium. One can see that up to three harmonics of the fundamental cavity frequency could be achieved.

Figure 24 shows the oscilloscope traces of the corresponding pulse trains with 1 (top), 2 and 3 pulses circulating in the cavity. The radio-frequency (RF) spectra of the mode-locked pulse trains are shown in Fig. 25. We find that harmonic modes exhibit nearly equal pulse-to-pulse spacings with large supermode suppression, >45 dB, in the RF spectrum. The hysteresis near the laser threshold, which may be expected from the abrupt power rise and indeed seen for other gain designs presented below (in Figs 27 and 29), could not be measured for this laser configuration. The switching between harmonics with hysteresis behavior was observed with a change in pump power or by blocking and unblocking the laser cavity. The size of the hysteresis loop

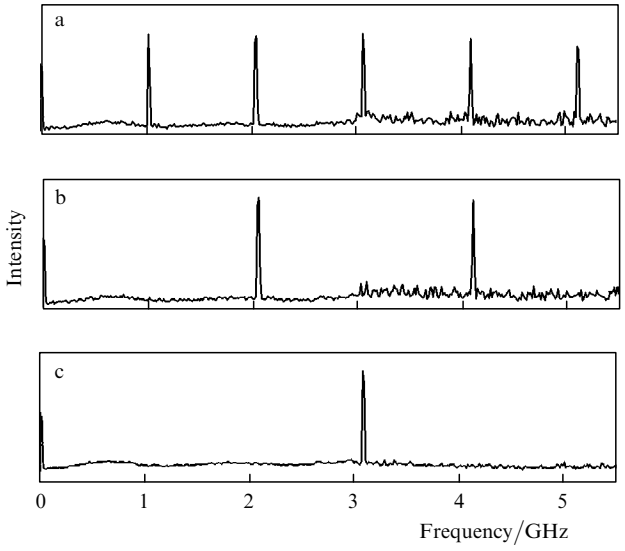

Figure 25. RF spectra of the pulse trains for the (a) fundamental, (b) second harmonic and (c) third harmonic state obtained with the RPG sample. Background noise depends slightly on the frequency range due to automatic switch in the sensitivity and averaging of the detection system of the RF analyser.

between the different harmonic states was, however, small, which can be attributed to the enhanced differential gain in the RPG medium resulting in an efficient rise in the unsaturable gain with pump power.

An interesting observation made during the experiments is that the laser could operate only in the mode-locked regime, i.e. other regimes, particularly continuous-wave oscillation, could be entirely avoided. This means that the lowest lasing threshold is always attained through mode-locked operation. A typical autocorrelation trace and a pulse spectrum for fundamental mode-locking at pump power of 0.84 W are shown in Fig. 26.

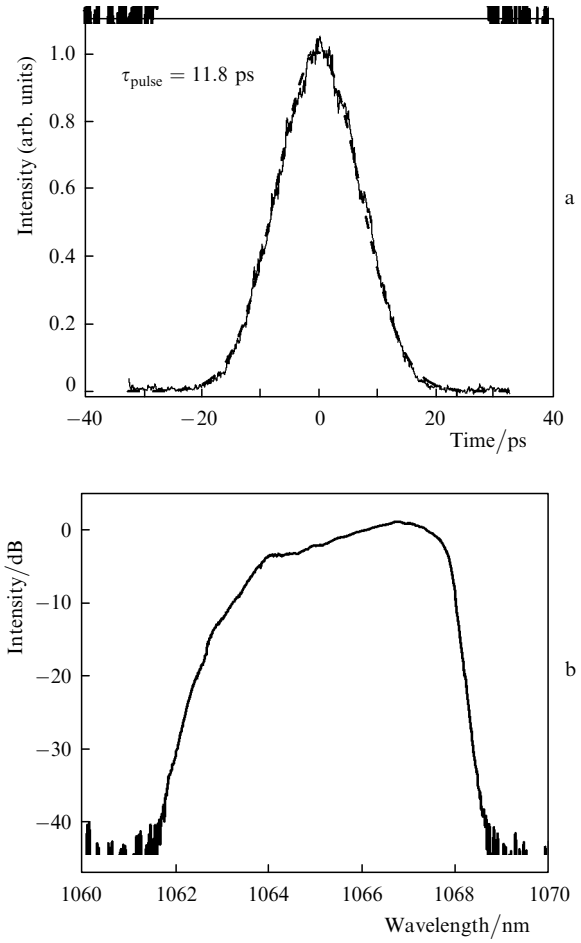

Figure 26. Pulse autocorrelation function (a) and pulse spectrum (b) for fundamental one-pulse mode-locking with pump power of 0.84 W.

One can see that the pulse is strongly chirped, which is a typical observation for mode-locked SDLs because of strong gain saturation and the consequent refractive index variation which causes a large nonlinear phase change [22, 26].

As expected, the hysteresis in the power characteristic was accompanied by hysteresis in the pulse duration and operation wavelength. Transition to a state with a higher harmonic number results in a decrease in the pulse energy and in consequent improvement of the pulse duration and quality, since the nonlinear distortions are less pronounced with a lower pulse energy [22, 26].

Next, to validate the role of the unsaturable gain in the hysteresis formation, the RPG sample, originally uncoated, was modified to reduce the gain enhancement due to the cavity effect. The reflectivity of the top surface was then decreased from 30 % to 5 % by applying a dielectric coating using an electron beam evaporator. The average output power for the coated RPG sample is plotted in Fig. 27 as a function of pump power. The figure shows that the loop size has increased substantially, indicating a reduction in the growth rate of unsaturable gain with pump power. Distinct hysteresis and bistability were also observed in the laser threshold when one-pulse mode-locking started from noise and turns off. Figure 28 shows pulse width and central wavelength for mode-locking states with one (fundamental) and two pulses circulating in the laser cavity.

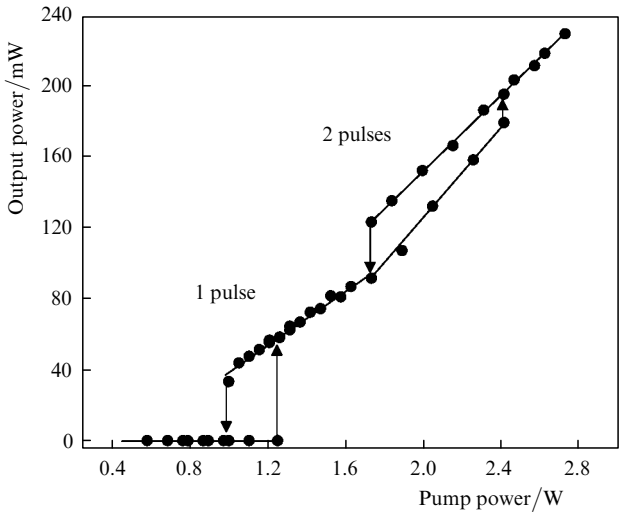

Figure 27. Output characteristics for the mode-locked disk laser using a resonant periodic gain medium with the top surface reflectivity reduced from 30 % for an uncoated sample to 5 % after dielectric film coating. The fundamental and the second harmonic have been achieved with a larger hysteresis loop compared to the uncoated sample presented in Fig. 23.

The characteristic hysteresis loops are clearly seen in the dependence of pulse width and wavelength on the pump power. The spectrum exhibits a gradual red shift when the pulse energy is increased with an increase in the pump power, owing to more complete average gain saturation, as seen in Fig. 28. However, there are 'blue abrupt hops' in the wavelength with an increase in the average output power corresponding to simultaneous increase in the number of pulses in the cavity. The effective step-like blue shifts with an increase in the number of pulses indicate a reduced red-shift in the gain medium because of less complete gain recovery between pulses with the higher repetition rate. The enlarged size of the hysteresis loop obtained with reduced gain enhancement due to the weaker cavity effect can be understood from a simple analysis based on the rate equations. Qualitatively, the reduced gain g and differential gain $\eta = \partial g/\partial P$ in a nonresonant medium result in an extended range of the pump power needed to reach the gain value required for start-up of mode-locking. Upon reduction in the pump power, the unsaturated gain decreases slowly owing to the small value of η resulting in a large hysteresis loop which extends to the point at which mode-locking and all laser action cease. Since the transient unsaturated gain associated with semiconductor laser mode-locking, with a further increase in pump power the gain continues to increase, and eventually the one-pulse regime

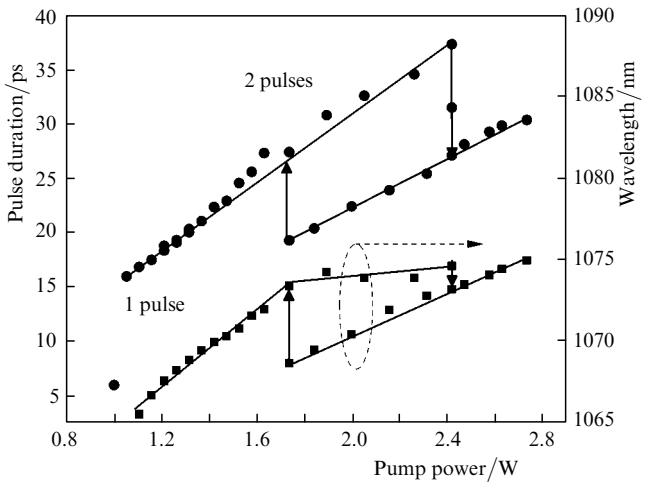

Figure 28. Pulse duration and operation wavelength for the coated RPG sample described in Fig. 27.

becomes unstable and mode-locking switches to a higher harmonic.

Finally, we study the performance of a laser exploiting alternative geometry of the active medium, the so-called antiresonant gain structure. The antiresonant gain structure comprises 5 InGaAs QWs placed in a 3.75λ-long gain section. The thickness of the InGaP etch-stop layer was increased from $\frac{1}{2}\lambda$ to $\frac{3}{4}\lambda$ to fulfill the antiresonance condition. Otherwise the antiresonant structure is similar to the RPG sample used before. After bonding, a two-layer TiO_2/Al_2O_3 coating producing a reflectivity of $\sim 10\,\%$ was applied to the surface of the sample.

Only operation at the fundamental frequency was observed for this laser for pump powers up to 3 W. The average output power and pulse duration are shown in Fig. 29 as a function of pump power. The hysteresis loop size and the corresponding bistability range are defined by the upper lasing threshold, when oscillation appears with an increase in the pump power, and the lower lasing threshold, when the lasing action stops with a decrease in the pumping rate. As expected, the value of the laser threshold for this

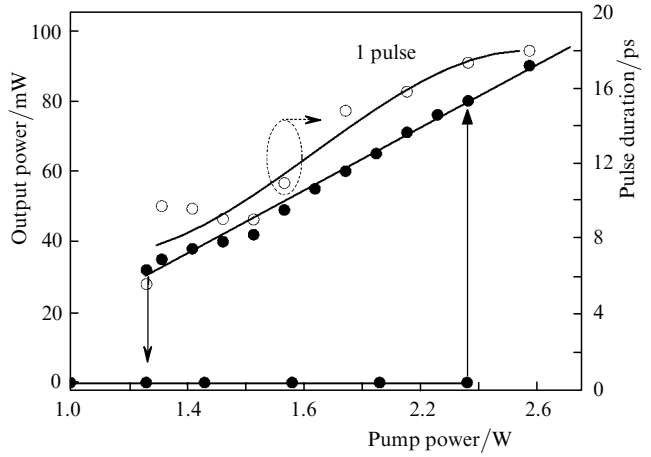

Figure 29. Output power and pulse duration for the mode-locked disk laser using an antiresonant gain medium design. A large hysteresis loop exhibiting a one-pulse state only has been observed with this laser configuration.

configuration is higher than for the resonant gain active media. Because the unsaturated gain growth rate is low in the antiresonant material, we could not observe the higher harmonics.

5. Conclusions

The optically-pumped semiconductor disk lasers have recently emerged as a promising version of semiconductor lasers. In contrast to conventional edge-emitting or vertical-cavity surface-emitting lasers, optically pumped SDL are rather similar to solid-state disk lasers. The ever growing pump power could not be entirely absorbed by a single gain element of the disk laser without an increase in the pump area. The solution based on the increase in the mode size is, however, limited since it is ultimately accompanied by a certain degradation of the beam quality. Dual-gain concept, presented here, allows to reduce the thermal load of the gain material, increase the threshold of rollover and extend capability for boosting the output power. Reduced thermal lensing also prevents the degradation in the beam quality. We have recognised that disk lasers could naturally adopt multigain cavity. With this geometry, the strong pump shared among gain media could be efficiently absorbed without the thermal overload. The output from a high-power pump source can be split into few beams to pump each gain structure separately. This geometry seems to be a promising solution for power scaling preserving the near diffraction-limited beam. The method allows for significant power improvement while preserving a good beam quality.

The dilute nitride GaInNAs quantum well material is known to provide high gain near 1.2 – 1.3 μm and take a full advantage of low-cost GaAs technology. An optically-pumped GaInNAs semiconductor disk lasers can therefore produce light in application-rich orange – red spectral range through intracavity second-harmonic generation. The SDL cavity is exceptionally appropriate for efficient intracavity frequency conversion. Recent results presented here validate the value of this approach by demonstration of 2.7 W at 612 nm with optical-to-optical conversion efficiency of 7.4 % and tuning range of 8-nm.

The presented results confirm the promising potential of SDLs as practical sources of high repetition rate ultrashort pulses. It is demonstrated that the strong pulse ordering mechanism in SDL due to the dynamic gain saturation allows for generation of highly periodical pulse trains at harmonics of fundamental frequency of the cavity crucial for many applications. We demonstrate experimental evidence of hysteresis with multiple pulse formation in the mode-locked regime of an optically-pumped semiconductor disk laser. Pulsed operation in the disk laser initiated with a semiconductor saturable absorber exhibits bistability of a single pulse or multiple pulse harmonic mode-locking dependent on the design of the semiconductor gain medium.

It should also be mentioned another mode-locking technique applied recently to SDL and presented here, i.e. synchronous pumping that allows one to improve an important figure of merit – timing jitter [31].

A bandwidth engineered emission wavelength of the SDL is an outstanding advantage that allows one to tailor significantly the accessible spectral range. The SDLs operating at 2 μm with watt-level output power have been demonstrated recently [33 – 35]. SDLs using gain media based on quantum-dot (QD) ensembles present an attractive

alternative to quantum-well semiconductors since they exhibit a broad gain spectrum and high temperature stability. Recently, we have demonstrated first QD-based SDL [36–38]. The research in this field could make an intrigue of the SDL development even more appealing.

To conclude, we have reviewed the key developments of SDLs and their state-of-the-art performance with a particular focus on power scaling, mode-locking and frequency-doubled devices emitting in the application-rich visible range. These devices show very attractive performance in robust configurations with a great deal of versatility. The SDL remains an exciting research area for the foreseeable future.

Acknowledgements. This research was supported in part by the European Commission through the FP6 research project NATAL. The author thanks J. Rautiainen, A. Härkönen, E. Saarinen, J. Lyytikäinen, R. Herda and M. Guina from Optoelectronics Research Centre, Tampere University of Technology.

References

1. Basov N.G., Bogdankevich O.V., Grasiuk A.Z. *IEEE J. Quantum Electron.*, **2**, 594 (1966).
2. Kuznetsov M., Hakimi F., Sprague R., Mooradian A. *IEEE J. Sel. Top. Quantum Electron.*, **5**, 561 (1999).
3. Giesen A., Speiser J. *IEEE J. Sel. Top. Quantum Electron.*, **13**, 598 (2007).
4. Raja M.Y.A., Brueck S.R.J., Osinski M., Schaus C.F., McInerney J.G., Brennan T.M., Hammons B.E. *IEEE J. Quantum Electron.*, **25**, 1500 (1989).
5. Lutgen S., Albrecht T., Brick P., Reill W., Luft J., Späth W. *Appl. Phys. Lett.*, **82**, 3620 (2003).
6. Härkönen A., Suomalainen S., Saarinen E., Orsila L., Koskinen R., Okhotnikov O., Calvez S., Dawson M. *IEE Electron. Lett.*, **42**, 693 (2006).
7. Hastie J.E., Hopkins J.-M., Calvez S., Jeon C.W., Burns D., Abram R., Riis E., Ferguson A.I., Dawson M.D. *IEEE Photon. Technol. Lett.*, **15**, 894 (2003).
8. Hastie J.E., Morton L.G., Calvez S., Dawson M.D., Leinonen T., Pessa M., Gibson G., Padgett M.J. *Opt. Express*, **13**, 7209 (2005).
9. Saarinen E., Härkönen A., Suomalainen S., Okhotnikov O.G. *Opt. Express*, **14**, 12868, (2006).
10. Stewen C., Contag K., Larionov M., Giesen A., Hugel H. *IEEE J. Sel. Top. Quantum Electron.*, **6**, 650 (2000).
11. Alford W.J., Raymond T.D., Allerman A.A. *J. Opt. Soc. Am. B*, **19**, 663 (2002).
12. Liau Z.L. *Appl. Phys. Lett.*, **77**, 651 (2000).
13. Fan L., Hsu T.-C., Fallahi M., Murray J.T., Bedford R., Kaneda Y., Hader J., Zakharian A.R., Moloney J.V., Koch S.W., Stolz W. *Appl. Phys. Lett.*, **88**, 251117 (2006).
14. Lee J.H., Lee S.M., Kim T., Park Y.J. *Appl. Phys. Lett.*, **89**, 241107 (2006).
15. Hilbich S., Seelert W.R., Ostroumov V.G., Kannengiesser C., von Elm R., Mueller J., Weiss E.S., Zhou H., Chilla J.L.A. *Proc. SPIE Int. Soc. Opt. Eng.*, **6451**, 64510C (2007).
16. Hastie J.E., Calvez S., Dawson D., Leinonen T., Laakso A., Lyytikäinen J., Pessa M. *Opt. Express*, **13**, 77 (2005).
17. Gerster E., Ecker I., Lorch S., Hahn C., Menzel S., Unger P. *J. Appl. Phys.*, **94**, 7397 (2003).
18. Hopkins J.-M., Smith S.A., Jeon C.W., Sun H.D., Burns D., Calvez S., Dawson M.D., Jouhti T., Pessa M. *Electron. Lett.*, **40**, 30 (2004).
19. Härkönen A., Rautiainen J., Guina M., Konttinen J., Tuomisto P., Orsila L., Pessa M., Okhotnikov O.G. *Opt. Express*, **15**, 3224 (2007).
20. Rautiainen J., Härkönen A., Tuomisto P., Konttinen J., Orsila L., Guina M., Okhotnikov O.G. *Electron. Lett.*, **43**, 980 (2007).
21. Rautiainen J., Härkönen A., Tuomisto P., Konttinen J., Orsila L., Guina M., Okhotnikov O.G. *Opt. Express*, **15**, 18345 (2007).
22. Hoogland S., Garnache A., Sagnes I., Roberts J.S., Tropper A.C. *IEEE Photon. Technol. Lett.*, **17**, 267 (2005).
23. Lorenser D., Unold H.J., Maas D.J.H.C., Aschwanden A., Grange R., Paschotta R., Ebling D., Gini E., Keller U. *Appl. Phys. A*, **79**, 927 (2004).
24. Zhang Q., Jasim K., Nurmikko A.V., Mooradian A., Carey G., Ha W., Ippen E. *IEEE Photon. Technol. Lett.*, **16**, 885 (2004).
25. Paschotta R., Häring R., Garnache A., Hoogland S., Tropper A.C., Keller U. *Appl. Phys. B*, **75**, 445 (2002).
26. Saarinen E., Herda R., Okhotnikov O.G. *Opt. Soc. Am. B*, **24**, 2784 (2007).
27. Mollenauer L.F., Stolen R.H. *Opt. Lett.*, **9**, 13 (1984).
28. Nathan Kutz J., Collings B., Bergman K., Knox W.H. *IEEE J. Quantum Electron.,* **34**, 1749 (1998).
29. Grudinin A.B., Richardson D.J., Payne D.N. *Electron. Lett.*, **28**, 1391 (1992).
30. Sanders S., Yariv A., Paslaski J., Ungar J.E., Zarem H.A. *Appl. Phys. Lett.*, **58**, 681 (1991).
31. Saarinen E.J., Lyytikäinen J., Okhotnikov O.G. *Phys. Rev. E*, **78**, 016207 (2008).
32. Saarinen E., Härkönen A., Herda R., Suomalainen S., Orsila L., Hakulinen T., Guina M., Okhotnikov O.G. *Opt. Express*, **15**, 955 (2007).
33. Härkönen A., Rautiainen J., Orsila L., Guina M., Röβner K., Hümmer M., Lehnhardt T., Müller M., Forchel A., Fischer M., Koeth J., Okhotnikov O.G. *IEEE Photon. Technol. Lett.*, **20**, 1332 (2008).
34. Härkönen A., Guina M., Okhotnikov O., Röβner K., Hummer M., Lehnhardt T., Müller M., Forchel A., Fischer M. *Opt. Express*, **14**, 6479 (2006).
35. Härkönen A., Guina M., Röβner K., Hümmer M., Lehnhardt T., Müller M., Forchel A., Fischer M., Koeth J., Okhotnikov O.G. *Electron. Lett.*, **43**, 457 (2007).
36. Germann T.D., Strittmatter A., Pohl J., Pohl U.W., Bimberg D., Rautiainen J., Guina M., Okhotnikov O.G. *Appl. Phys. Lett.*, **91**, 101123 (2008).
37. Germann T.D., Strittmatter A., Pohl J., Pohl U.W., Bimberg D., Rautiainen J., Guina M., Okhotnikov O.G. *Electron. Lett.*, **44**, 290 (2008).
38. Germann T.D., Strittmatter A., Pohl J., Pohl U.W., Bimberg D., Rautiainen J., Guina M., Okhotnikov O.G. *Appl. Phys. Lett.*, **93**, 051104 (2008).